Hindawi Publishing Corporation
International Journal of Corrosion
Volume 2015, Article ID 386865, 9 pages
http://dx.doi.org/10.1155/2015/386865

Research Article

Effects of Strain Energy and Grain Size on Corrosion Resistance of Ultrafine Grained Fe-20%Cr Steels with Extremely low C and N Fabricated by ECAP

Muhammad Rifai,[1] Hiroyuki Miyamoto,[2] and Hiroshi Fujiwara[2]

[1]*Graduate School of Science and Engineering, Doshisha University, 1-3 Tatara Miyakodani, Kyotanabe, Kyoto 610-0394, Japan*
[2]*Department of Mechanical Engineering, Doshisha University, 1-3 Tatara Miyakodani, Kyotanabe, Kyoto 610-0394, Japan*

Correspondence should be addressed to Muhammad Rifai; eum1504@mail4.doshisha.ac.jp

Received 26 August 2014; Revised 9 November 2014; Accepted 21 December 2014

Academic Editor: Raman Singh

Effect of strain energy and grain size on corrosion resistance of ultrafine grained (UFG) Fe-20%Cr steels with extremely low C and N fabricated by equal channel angular pressing (ECAP) was investigated. UFG structures of initial grain size of 144 nm exhibited the typical three-stage softening comprising recovery, recrystallization, and grain growth. Potentiodynamic polarization measurements were carried out with a conventional three-electrode cell to evaluate pitting potential. Pitting potential in 1000 mol·m^{-3} NaCl solution was nobler in UFG state, but pitting potential started to decrease monotonously at lower temperature compared to hardness. The degradation of corrosion resistance in the early stage of annealing is attributed to stability change of passivation by recovery of dislocation structures inside grains and in nonequilibrium grain boundaries. We therefore conclude that nobler potentials of UFG states were realized by not only grain size reduction but also defective deformation-induced UFG.

1. Introduction

Severe plastic deformation (SPD) is now recognized as a process to fabricate nanocrystalline or ultrafine grain (UFG) metallic materials in a bulk form [1]. Deformation-induced nanocrystalline or UFG materials by SPD exhibit high strength with smaller sacrifice of ductility [1, 2]. Since SPD does not require an alloying element for strengthening, it is also expected to become an important processing for structural application. Microstructural development and resultant deformation-induced grain subdivision during SPD have been of interest from scientific and practical standpoints and have extensively been studied with mechanical and physical properties in the last 20 years [1, 3–5]. Corrosion properties are also important for structural application. The beneficial effect of grain size reduction to the nanoscale was first demonstrated for intergranular corrosion in electrodeposited nanocrystalline nickel thanks to the pioneering work of Rofagha et al. [6], Kim et al. [7, 8], followed by Mahesh and Raman [9]. They observed a rather smooth surface with a smaller penetration rate at grain boundaries and thus considerable improvement in intergranular corrosion. For SPD materials, corrosion behavior such as general [10–20], intergranular [21–23] and pitting corrosion [21, 24–32] of UFG aluminum and aluminum alloy [17, 21, 22, 24, 25, 29–32], copper and copper alloy [11, 15, 19, 28] as well as stainless steels [10, 12, 18, 23, 27] and magnesium [13, 14, 16, 20] processed by SPD, and corrosive environment dependence [33–35] have been reported. For example, corrosion resistance of aluminum alloys has mostly been reported to improve by UFG formation by SPD [17, 21, 25, 29, 30] and is attributed to (1) fragmentation of a precipitation or second phase which tends to be pitting sites [17, 21, 25, 29, 30], and (2) dissolution of precipitation forming supersaturation. When the precipitation becomes smaller than critical size, it does not work as cathode site for pitting formation [30]. For Fe-Cr steels in which passivation occurs by Cr elements, pitting corrosion resistance is enhanced by UFG formation by SPD

because Cr diffusion to the surface is enhanced by the high density of dislocations and grain boundaries and promotes passivation [12, 27, 36, 37].

UFG metals by SPD exhibit unique mechanical and physical properties. Deformation-induced nanocrystalline or UFG structure with stored dislocations and nonequilibrium grain boundaries are considered to cause these unique properties. For example, Huang et al. [39] reported that UFG aluminum fabricated by accumulative roll bonding (ARB) becomes harder by post-ARB annealing and softer by subsequent deformation. The present authors reported [11] that corrosion resistance of UFG copper was inferior to coarse grain counterparts but was improved by short-time postequal channel angular pressing (ECAP) annealing without accompanying grain size change. This improvement is attributed to the grain boundary structural change from nonequilibrium to equilibrium state. Since nonequilibrium grain boundaries comprise the extrinsic grain boundary dislocations [1], mechanical, physical, and chemical properties should be affected [1]. However, corrosion properties have not been well studied from this viewpoint as compared with mechanical properties. In the present study, the effects of post-ECAP annealing on pitting corrosion of UFG Fe-20%Cr steels with extremely low C and N are investigated focusing on the structural transition which may occur during the annealing process.

2. Experimental Procedure

2.1. Material. The material used in this experiment has a chemical composition of UFG Fe-20%Cr steels with extremely low C and N with Cr; 20.03, C; 0.0004, N; 0.0013, and Fe balance (in mass percent). Measurement of chemical composition of the material was carried out by Nitetsu Sumikin Technology Co., Ltd. A chemical analysis of C, Cr, and N contents was performed by infrared absorption spectroscopy, inductively coupled plasma emission spectrometry, and inert gas fusion method, respectively.

2.2. Sample Processing. This material was machined with dimensions of 8 × 8 × 100 mm for ECAP pressing. ECAP procedures are carried out up to 8 passes at 423 K via the so-called route Bc using a split die with two channels intersecting at an inner angle of 90°. The samples are lubricated with high temperature fluorine lubricating grease. After ECAP, billets were annealed using infrared furnace (ULVAC MILA5000) from 473 to 1373 K in a vacuum for one hour. A corrosion testing specimen was prepared from an ECAPed sample using a spark-erosion machine. The specimen was in the shape of a square with an area of 8 mm × 6 mm and a thickness of 2 mm. This specimen was soldered with a connection cable on the back side of the surface of the corrosion and then coated with epoxy molding to cover the connection. The edge area was sealed with tape to prevent any corrosion due to the edge effect of pitting corrosion. The mounted specimen was ground with abrasive papers from number 240 until number 2000 and then polished with buff paper with alumina suspension (PRESI) 9 μm, 3 μm, and 1 μm. For the last step of the polishing process, an OP-S suspension (Struers) was used.

2.3. Microhardness. The microhardness experiments were performed on a Vickers hardness testing machine under a load, for 15 s dwell time after each annealing. Hardness testing was carried out for ten times per each sample.

2.4. Microstructural Characterization. A scanning electron microscope of field-emission type (FE-SEM, JSM 7001F), equipped with electron back-scattered diffraction (EBSD, Oxford Instrument Co.) image was used to observe orientation map of grains. EBSD orientation maps were processed using INCA software.

A field-emission transmission electron microscope (FE-TEM, JEM 2100F) was used to examine the microstructures. Thin foils for TEM were polished using abrasive papers to about 100 μm thick and then thinned by a twin-jet polishing Tenupol 5 facility (Struers Co., Ltd.) using a solution of 40% acetic acid, 30% phosphoric acid, 20% nitric acid, and 10% distilled water.

2.5. X-Ray Diffraction. X-ray diffraction (XRD) on ECAPed and postannealed sample was carried out by SmartLab, Rigaku. XRD sample surfaces were buffed by an automatic polisher. The SmartLab X-ray diffractometer used CuKα, 40 kV, and 0.2 A from 30 until 120 deg with continuous scanning type. Full width half maximum (FWHM) was determined after fitting the scattered XRD data.

2.6. Electrochemical Testing. The specimen for pitting corrosion testing is shown in Figure 1. Pitting corrosion testing was carried out in neutral solutions of 1000 mol·m^{-3} NaCl at room temperature by dynamic anodic polarization, using a potentiostat (HOKUTO H100) at a scan rate of 20 mV/min, a corrosion current, and an Ag/AgCl reference electrode were recorded by a data logger. Ag/AgCl electrode reference was put in 3000 mol·m^{-3} KCl (potassium chloride solution saturated) for three times. This pitting testing arrangement is shown in Figure 2. Before pitting corrosion testing was carried out, argon gas was used to remove dissolved oxygen. The testing process was initialized after the open circuit potential (OCP) of the specimen was stabilized. The polarization was started from 50 mV lower than the OCP after immersion in the test solution for 5 minutes.

The potential at which the passivation starts to break down at localized areas, leading to pitting, is defined as the pitting potential. Pitting potential can be determined from the anodic polarization curve as the potential at which the current starts to sharply rise with increasing potential [38] and pitting potential was defined accordingly as shown in Figure 3. The pitting potential of as received specimen was −0.033 V versus Ag/AgCl.

3. Results

3.1. Microhardness. Vickers hardness of after the post-ECAP annealing at temperature ranging from 473 to 1373 K was

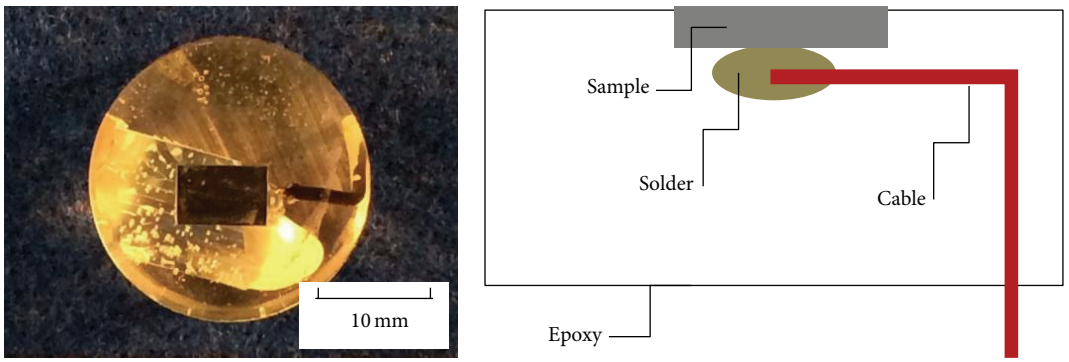

Figure 1: (a) Pitting testing specimen and (b) schema of specimen (electric conduction).

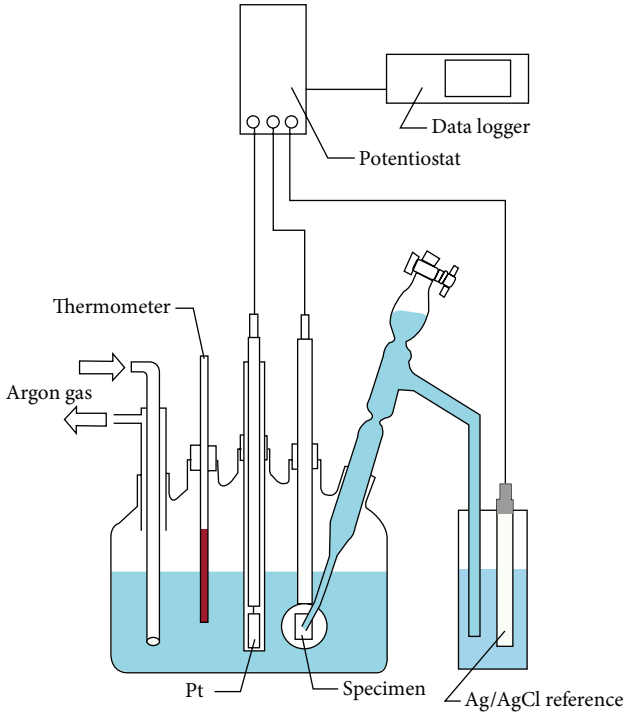

Figure 2: Schematic of pitting testing equipment arrangement.

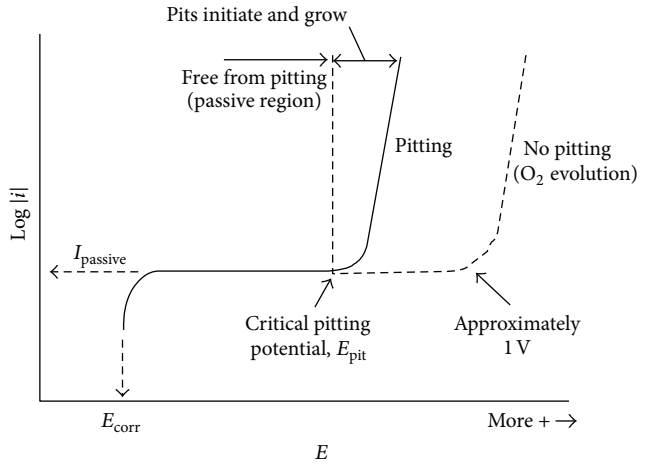

Figure 3: Schematic anodic polarization curve showing the critical pitting potential (for a passive metal) [38].

shown in Figure 4. The hardness exhibited the typical three-stages softening. Namely, the hardness remained relatively constant after the annealing at temperature up to 698 K and then declined considerably until the temperature of 973 K. The hardness remained constant again at higher temperature. In the general interpretation of this softening behavior, the recovery process might proceed accompanying dislocation rearrangement and annihilation in the first stage where the hardness remains relatively constant, followed by the recrystallization which accompanies the noticeable softening in the second stage and grain growth of constant hardness again as the third stage.

3.2. Microstructural Characterization. Orientation image maps by EBSD after the post-ECAP annealing are shown

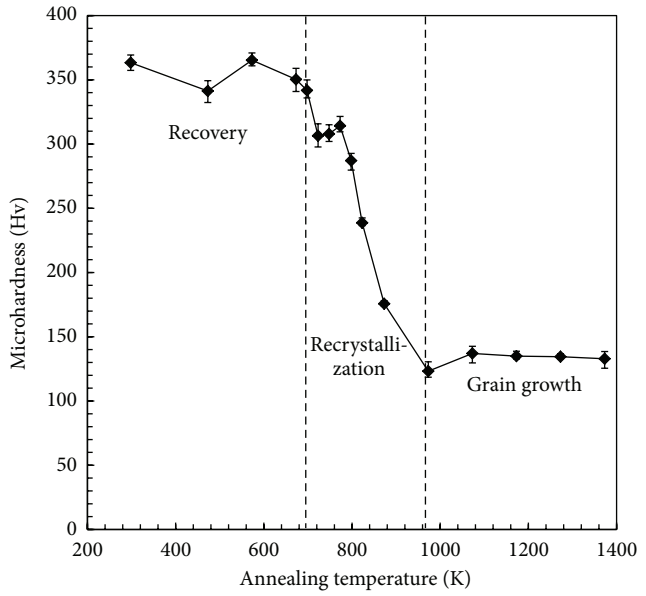

Figure 4: Effect of the post-ECAP annealing temperature on Vickers hardness.

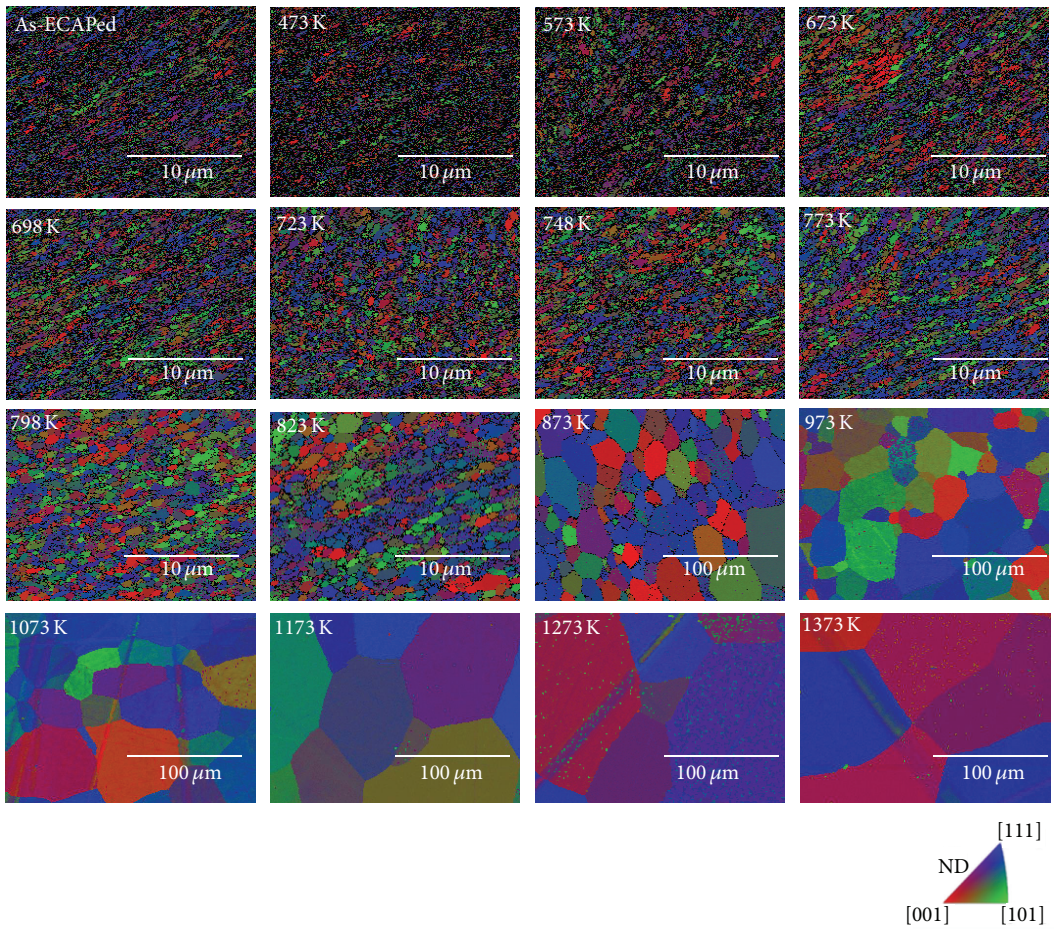

Figure 5: Color orientation image maps obtained by EBSD after the post-ECAP annealing.

in Figure 5. UFG structure of grain size less than 200 nm can be recognized in as-ECAPed state, and the grain size remained constant in the first stage at temperature up to 698 K. In the second stage from 698 to 973 K, where significant softening occurred, uniform grain growth was observed. This uniform grain growth during post-ECAP annealing is contrasted with those observed in face-centered cubic (FCC) metals such as copper [40–43], nickel [33, 43], and austenitic stainless steels [44] where a small fraction of grains grow preferentially, replacing the other smaller grains. This inhomogeneous microstructural coarsening observed in FCC metals is similar to abnormal grain growth and can be viewed also as nucleation and the grain growth process in the discontinuous recrystallization [40, 45]. In body-centered cubic (BCC) metals, on the other hand, strain energy stored as dislocations can be easily released in the recovery process prior to recrystallization. Therefore, strain energy stored in UFG structures in as-ECAP state was possibly released prior to the next stage, resulting in the formation of UFG with less stored strain energy. Uniform grain size distribution with a high fraction of high angle grain boundaries may lead to uniform grain growth whose driving force is solely grain boundary energy [46], rather than the nucleation-growth mode of restoration which requires strain energy as a driving force.

The microhardness indenter appearance and Hall-Petch (HP) relation for annealed UFG specimens can be seen in Figure 6. The linear fit was applied only to data corresponding to annealing temperatures from 298 to 823 K. In high temperature range, only the grain size affects material hardness as the dislocation density is high. At low temperatures, both grain size and dislocation density contribute to strengthening and the linear fit of microhardness data.

Figure 7 shows TEM micrographs of as-ECAPed and after post-ECAP annealing at 698 K. If one compares two micrographs, the grain sizes are essentially the same and little difference is recognized. However, more detailed observation revealed some grains with darker contrast in the as-ECAPed state, which indicate that dislocation occurred within grains. This suggests that some fraction of dislocations stored by SPD was released by the post-ECAP annealing. Figure 8 shows X-ray {110} diffraction after ECAP and the annealing. In as-ECAP state, significant line broadening can be observed, which is a result of nonequilibrium grain boundaries with a high density of extrinsic defects in their structure and resultant long-range elastic stresses [47, 48]. After the annealing this line broadening becomes sharper with increasing

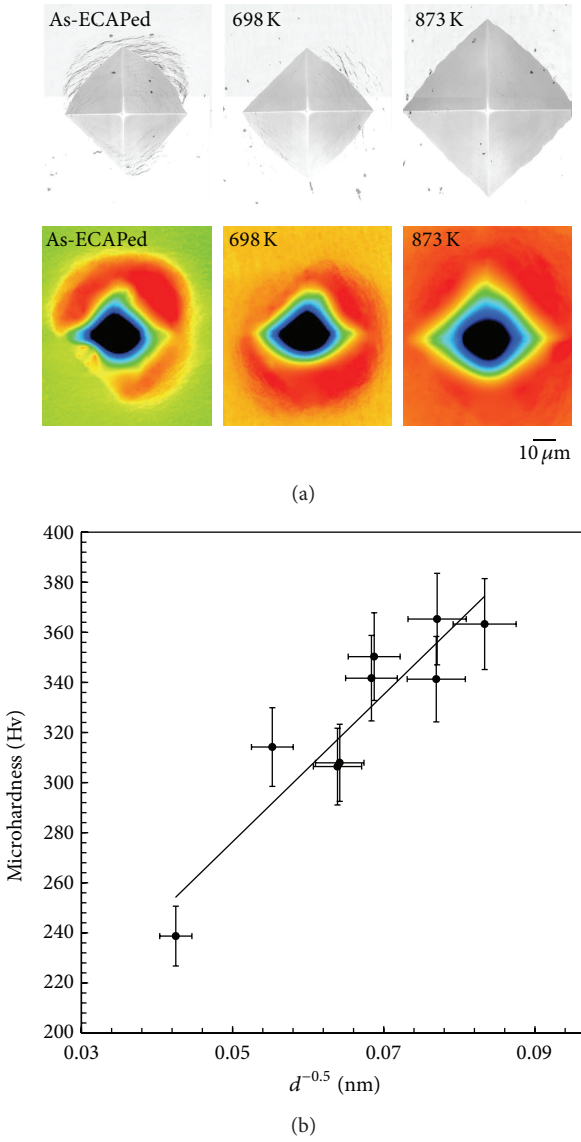

Figure 6: (a) Indenter appearance of Vickers hardness and (b) relationship between hardness and grain size.

temperature. Thus, the parameter X is defined as a measure of the structural change during the annealing as follows:

$$X = \frac{(W_i - W_r)}{(W_d - W_r)}, \quad (1)$$

where W_i is the width of the peak at half height at temperatures T_i and W_r and W_d are those in recrystallized and deformed state, respectively. Figure 9 shows the variation of X parameter as a function of annealing temperature. Note that the parameter X started to decrease monotonously at lower temperature compared to hardness as shown in Figure 4. This early reduction of X was reported in pure iron [49] and can be interpreted as follows: (1) the partial annihilation of stored dislocations by the recovery process, which is fast in BCC as compared with FCC metals because of easy cross-slip of screw dislocations; and (2)

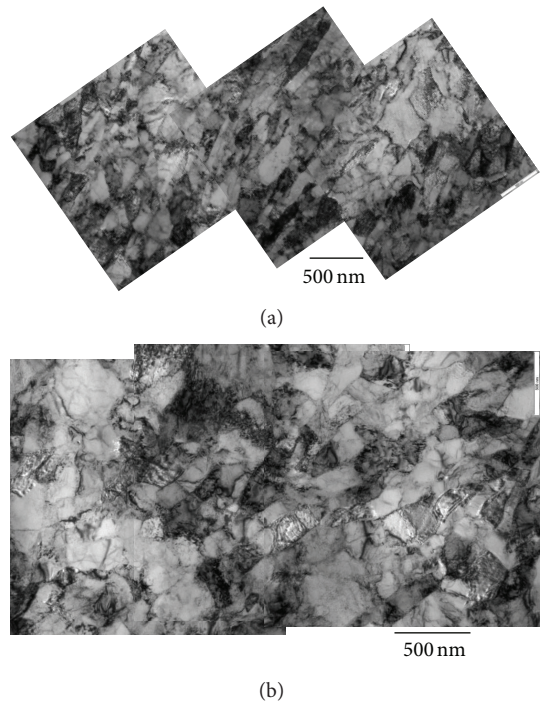

Figure 7: TEM micrographs (a) after eight passes ECAP and (b) after post-ECAP annealing at 698 K.

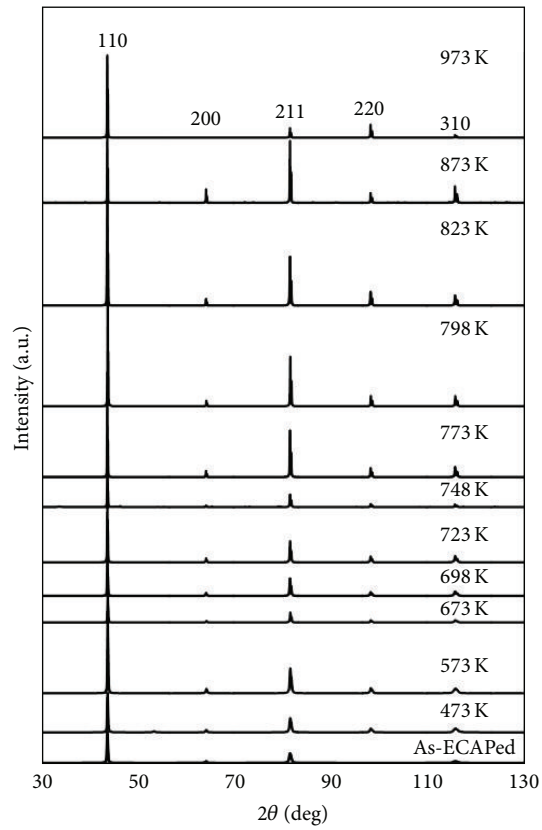

Figure 8: X-ray {110} diffractions after ECAP and annealing.

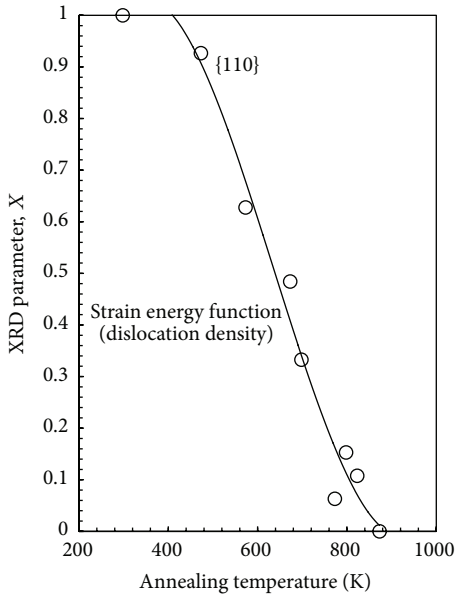

FIGURE 9: X-ray parameter as a function of the post-ECAP annealing temperature.

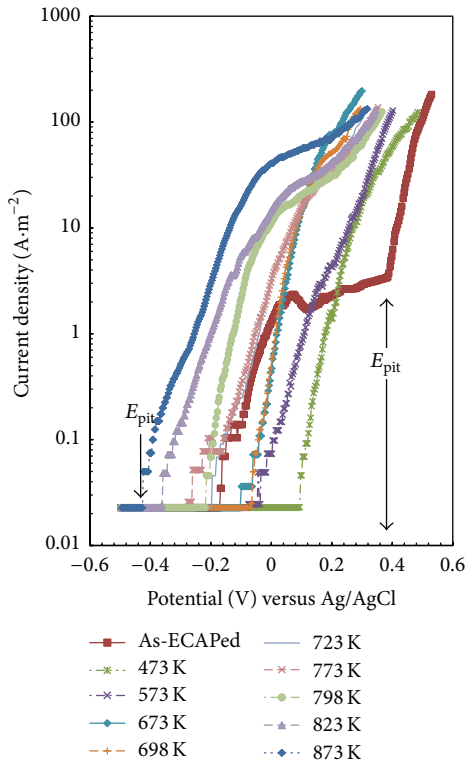

FIGURE 10: Dynamic anodic polarization curves in 1000 mol·m^{-3} NaCl solution.

change from nonequilibrium grain boundaries to equilibrium grain boundaries and relaxation of internal elastic stress. Since nonequilibrium grain boundaries have extrinsic grain boundary dislocations, they cause a stress field in the grain interior. The annihilation and rearrangement of extrinsic dislocations result in the relaxation of internal elastic stress [47, 48].

3.3. Electrochemical Properties. Resistance to pitting corrosion is investigated by dynamic anodic polarization tests as shown in Figure 10. As typical anodic behavior, anodic current stayed at relatively constant level and increased abruptly at a nobler potential compared to a critical value where pitting started to form. Only as-ECAPed state exhibited anomalous two-stage development prior to pitting. This high anodic current at passive region in as-ECAPed state may be associated with defective passive film formed on the surface with high grain boundaries and dislocation density. Pitting potential, E_p versus Ag/AgCl, increased with annealing temperature as shown in Figure 11(a). If E_p versus Ag/AgCl is plotted as a function of the parameter X, then these two have linear relation (Figure 11(b)). Pitting corrosion was confirmed from laser microscope observations, which showed that larger and more pitting corrosion occurred after annealing process as shown in Figure 12.

4. Discussion

Pitting stainless steel is a type of corrosion in which the chromium in the passive layer is dissolved removing iron. Pitting is localized attack that can produce penetration of a stainless steel with weight loss to the total structure. It is related to a local discontinuity of the passive film. It can be a mechanical imperfection, such as an inclusion or surface damage, or it can be a local chemical breakdown of the film [50]. Once a pit is formed, it in effect becomes a crevice; the local chemical environment is substantially more aggressive than the bulk environment [50]. This explains why very high flow rates over a stainless steel surface tend to reduce pitting corrosion; the high flow rate prevents the concentration of corrosive species in the pit [50].

The chemical composition of the alloy plays a major role in affecting the pitting potential. In stainless steels, chromium is the main alloying element required to improve the pitting resistance. Increasing chromium content enhanced the stability of the passive film against pitting attack. The pitting potential was correspondingly found to increase dramatically as the chromium content increased above the critical 13% needed to create stainless steel [51].

The effect of grain size on pitting potential can be seen in Figure 13. This pitting corrosion testing exhibited low rates of corrosion or some level of passivity corrosion rated decreased with grain size reduction. This occurrence is coherent with pure grain refinement being principally confined to controlling the rate of anodic reactions and having little role in altering the rate at which cathodic reactions can be sustained [52].

Resistance to corrosion of stainless steel was reportedly enhanced by UFG formation by SPD [27, 36, 37]. This is often explained by the higher diffusion of Cr enhanced by high density of grain boundaries [53–55]. The higher diffusion of Cr is explained by the fact that the passive film forms

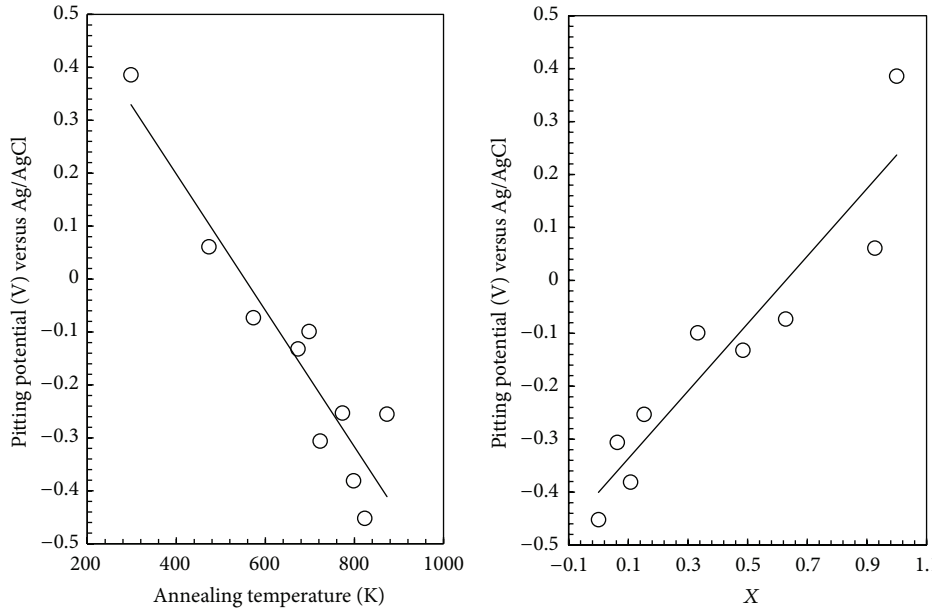

FIGURE 11: Relation between, (a) the pitting potential, E_p and annealing temperature and (b) X parameter.

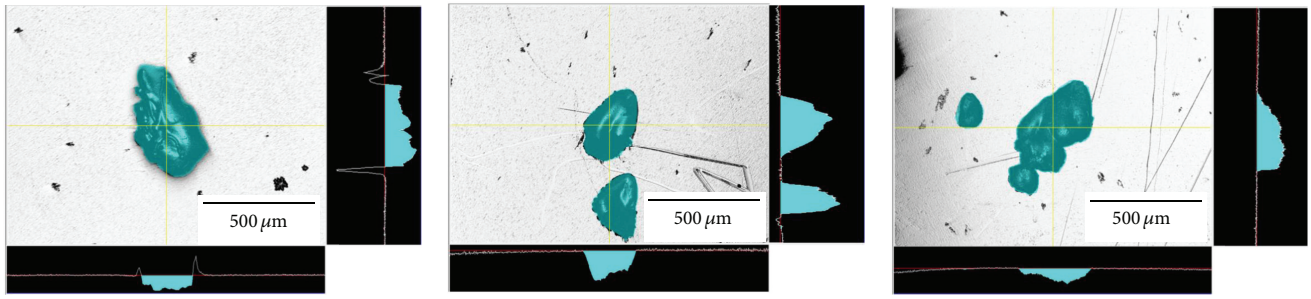

FIGURE 12: Laser microscope showing pitting corrosion of (a) as-ECAPed, (b) annealed at 573 K, (c) 773 K.

by selective dissolution of Fe atoms into the solution and resultant enrichment of Cr at the surface [56, 57]. When pitting started to form, the Cr concentration decreased locally, but this area would be supplied by enhanced Cr diffusion in UFG structures. If one can apply this idea to the present results, the linear relation of X and E_p versus Ag/AgCl can be interpreted by the faster diffusion of Cr along the stored dislocations inside the grains or/and nonequilibrium grain boundaries [58, 59]. Indeed, it has been shown that the grain boundary diffusivities in nanostructured metals processed by means of severe plastic deformation in the temperature range of 398–448 K are 4-5 orders of magnitude higher relative to the same materials in a coarse-grained state [58]. Namely, early reduction of E_p versus Ag/AgCl by the annealing can be caused by diminishing dislocations or transformation from nonequilibrium to equilibrium grain boundaries. Gutman suggested that dislocation arrangements during the strain hardening stages could better explain this trend according to electrochemical approaches [60].

5. Summary

Effect of post-ECAP annealing on the pitting corrosion of UFG Fe-20%Cr steels with extremely low C and N fabricated by ECAP was studied. It was found that softening occurred by the typical three-stage change comprising of recovery with constant hardness and subsequent recrystallization accompanying significant softening and the final grain growth with constant hardness. Pitting potential was nobler in UFG state and more sensitive to annealing temperature than hardness. Namely, pitting potential started to decrease monotonously at a lower temperature than the hardness which reflected grain size change. The early reduction of the pitting potential in the recovery process is attributed to the less stabilized passivation caused by the rearrangement and annihilation of dislocations inside grains and in nonequilibrium grain boundaries. We conclude that nobler potentials of UFG states are realized by not only grain size reduction but also defective deformation-induced UFG.

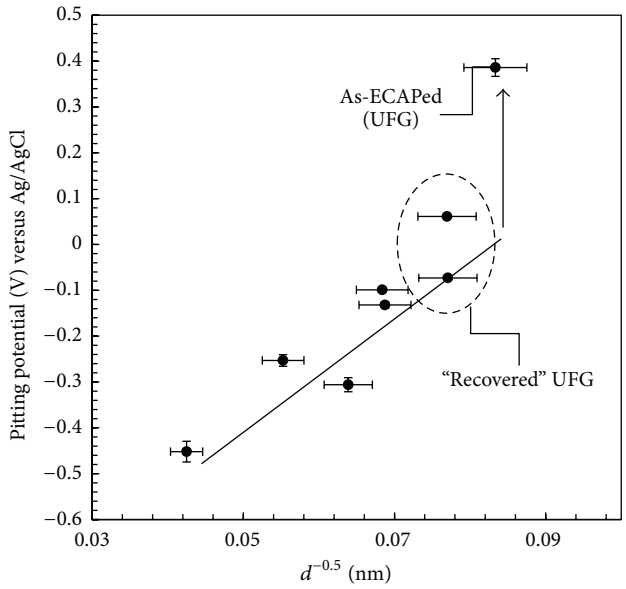

Figure 13: Relationship between pitting potential (V) versus Ag/AgCl and microhardness.

Conflict of Interests

The authors declare that there is no conflict of interests regarding the publication of this paper.

References

[1] R. Z. Valiev, R. K. Islamgaliev, and I. V. Alexandrov, "Bulk nanostructured materials from severe plastic deformation," *Progress in Materials Science*, vol. 45, no. 2, pp. 103–189, 2000.

[2] C. C. Koch, "Optimization of strength and ductility in nanocrystalline and ultrafine grained metals," *Scripta Materialia*, vol. 49, no. 7, pp. 657–662, 2003.

[3] T. G. Langdon, "The principles of grain refinement in equal-channel angular pressing," *Materials Science and Engineering A*, vol. 462, no. 1-2, pp. 3–11, 2007.

[4] T. G. Langdon, "Twenty-five years of ultrafine-grained materials: achieving exceptional properties through grain refinement," *Acta Materialia*, vol. 61, no. 19, pp. 7035–7059, 2013.

[5] Y. T. Zhu and T. C. Lowe, "Observations and issues on mechanisms of grain refinement during ECAP process," *Materials Science and Engineering A*, vol. 291, no. 1, pp. 46–53, 2000.

[6] R. Rofagha, R. Langer, A. M. El-Sherik, U. Erb, G. Palumbo, and K. T. Aust, "The corrosion behaviour of nanocrystalline nickel," *Scripta Metallurgica et Materiala*, vol. 25, no. 12, pp. 2867–2872, 1991.

[7] S. H. Kim, K. T. Aust, U. Erb, F. Gonzalez, and G. Palumbo, "A comparison of the corrosion behaviour of polycrystalline and nano crystalline cobalt," *Scripta Materialia*, vol. 48, no. 9, pp. 1379–1384, 2003.

[8] S. H. Kim, U. Erb, K. T. Aust, F. Gonzalez, and G. Palumbo, "The corrosion behavior of nanocrystalline electrodeposits," *Plating and Surface Finishing*, vol. 91, no. 5, pp. 68–70, 2004.

[9] B. V. Mahesh and R. S. Raman, "Role of nanostructure in electrochemical corrosion and high temperature oxidation: a review," *Metallurgical and Materials Transactions A*, vol. 45, no. 12, pp. 5799–5822, 2014.

[10] M. Hasegawa and M. Osawa, "Corrosion behavior of ultrafine grained austenitic stainless steel," *Corrosion*, vol. 40, no. 7, pp. 371–374, 1984.

[11] H. Miyamoto, K. Harada, T. Mimaki, A. Vinogradov, and S. Hashimoto, "Corrosion of ultra-fine grained copper fabricated by equal-channel angular pressing," *Corrosion Science*, vol. 50, no. 5, pp. 1215–1220, 2008.

[12] T. Balusamy, S. Kumar, and T. S. N. S. Narayanan, "Effect of surface nanocrystallization on the corrosion behaviour of AISI 409 stainless steel," *Corrosion Science*, vol. 52, no. 11, pp. 3826–3834, 2010.

[13] G. B. Hamu, D. Eliezer, and L. Wagner, "The relation between severe plastic deformation microstructure and corrosion behavior of AZ31 magnesium alloy," *Journal of Alloys and Compounds*, vol. 468, no. 1-2, pp. 222–229, 2009.

[14] N. Birbilis, K. D. Ralston, S. Virtanen, H. L. Fraser, and C. H. J. Davies, "Grain character influences on corrosion of ECAPed pure magnesium," *Corrosion Engineering Science and Technology*, vol. 45, no. 3, pp. 224–230, 2010.

[15] X. X. Xu, F. L. Nie, J. X. Zhang et al., "Corrosion and ion release behavior of ultra-fine grained bulk pure copper fabricated by ECAP in Hanks solution as potential biomaterial for contraception," *Materials Letters*, vol. 64, no. 4, pp. 524–527, 2010.

[16] D. Orlov, K. D. Ralston, N. Birbilis, and Y. Estrin, "Enhanced corrosion resistance of Mg alloy ZK60 after processing by integrated extrusion and equal channel angular pressing," *Acta Materialia*, vol. 59, no. 15, pp. 6176–6186, 2011.

[17] J. Jiang, A. Ma, D. Song et al., "Anticorrosion behavior of ultrafine-grained Al-26 wt% Si alloy fabricated by ECAP," *Journal of Materials Science*, vol. 47, no. 22, pp. 7744–7750, 2012.

[18] Z. J. Zheng, Y. Gao, Y. Gui, and M. Zhu, "Corrosion behaviour of nanocrystalline 304 stainless steel prepared by equal channel angular pressing," *Corrosion Science*, vol. 54, no. 1, pp. 60–67, 2012.

[19] W. Deng, P. Lin, Q. Li, and G. Mo, "Ultrafine-grained copper produced by machining and its unusual electrochemical corrosion resistance in acidic chloride pickling solutions," *Corrosion Science*, vol. 74, pp. 44–49, 2013.

[20] J. Vrátná, B. Hadzima, M. Bukovina, and M. Janeček, "Room temperature corrosion properties of AZ31 magnesium alloy processed by extrusion and equal channel angular pressing," *Journal of Materials Science*, vol. 48, no. 13, pp. 4510–4516, 2013.

[21] J. G. Brunner, N. Birbilis, K. D. Ralston, and S. Virtanen, "Impact of ultrafine-grained microstructure on the corrosion of aluminium alloy AA2024," *Corrosion Science*, vol. 57, pp. 209–214, 2012.

[22] K. Gopala Krishna, K. Sivaprasad, T. S. N. Sankara Narayanan, and K. C. Hari Kumar, "Localized corrosion of an ultrafine grained Al-4Zn-2Mg alloy produced by cryorolling," *Corrosion Science*, vol. 60, pp. 82–89, 2012.

[23] A. T. Krawczynska, M. Gloc, and K. Lublinska, "Intergranular corrosion resistance of nanostructured austenitic stainless steel," *Journal of Materials Science*, vol. 48, no. 13, pp. 4517–4523, 2013.

[24] E. Sikora, X. J. Wei, and B. A. Shaw, "Corrosion behavior of nanocrystalline bulk Al-Mg-based alloys," *Corrosion*, vol. 60, no. 4, pp. 387–398, 2004.

[25] M.-K. Chung, Y.-S. Choi, J.-G. Kim, Y.-M. Kim, and J.-C. Lee, "Effect of the number of ECAP pass time on the electrochemical

properties of 1050 Al alloys," *Materials Science and Engineering A*, vol. 366, no. 2, pp. 282–291, 2004.

[26] B. Hadzima, M. Janeček, Y. Estrin, and H. S. Kim, "Microstructure and corrosion properties of ultrafine-grained interstitial free steel," *Materials Science and Engineering A*, vol. 462, no. 1-2, pp. 243–247, 2007.

[27] M. Pisarek, P. Kedzierzawski, M. Janik-Czachor, and K. J. Kurzydłowski, "Effect of hydrostatic extrusion on the corrosion resistance of type 316 stainless steel," *Corrosion*, vol. 64, no. 2, pp. 131–137, 2008.

[28] R. J. Hellmig, M. Jancček, B. Hadzima et al., "A portrait of copper processed by equal channel angular pressing," *Materials Transactions*, vol. 49, no. 1, pp. 31–37, 2008.

[29] M. Hockauf, L. W. Meyer, D. Nickel et al., "Mechanical properties and corrosion behaviour of ultrafine-grained AA6082 produced by equal-channel angular pressing," *Journal of Materials Science*, vol. 43, no. 23-24, pp. 7409–7417, 2008.

[30] E. Akiyama, Z. Zhang, Y. Watanabe, and K. Tsuzaki, "Effects of severe plastic deformation on the corrosion behavior of aluminum alloys," *Journal of Solid State Electrochemistry*, vol. 13, no. 2, pp. 277–282, 2009.

[31] J. G. Brunner, J. May, H. W. Höppel, and S. Virtanen, "Localized corrosion of ultrafine-grained Al-Mg model alloys," *Electrochimica Acta*, vol. 55, no. 6, pp. 1966–1970, 2010.

[32] A. Korchef and A. Kahoul, "Corrosion behavior of commercial aluminum alloy processed by equal channel angular pressing," *International Journal of Corrosion*, vol. 2013, Article ID 983261, 11 pages, 2013.

[33] B. Yu, P. Woo, and U. Erb, "Corrosion behaviour of nanocrystalline copper foil in sodium hydroxide solution," *Scripta Materialia*, vol. 56, no. 5, pp. 353–356, 2007.

[34] W. Zeiger, M. Schneider, D. Scharnweber, and H. Worch, "Corrosion behaviour of a nanocrystalline FeA18 alloy," *Nanostructured Materials*, vol. 6, pp. 1013–1016, 1995.

[35] V. Afshari and C. Dehghanian, "Effects of grain size on the electrochemical corrosion behaviour of electrodeposited nanocrystalline Fe coatings in alkaline solution," *Corrosion Science*, vol. 51, no. 8, pp. 1844–1849, 2009.

[36] R. K. S. Raman, R. K. Gupta, and C. C. Koch, "Resistance of nanocrystalline vis-à-vis microcrystalline Fe-Cr alloys to environmental degradation and challenges to their synthesis," *Philosophical Magazine*, vol. 90, no. 23, pp. 3233–3260, 2010.

[37] B. V. Mahesh, R. K. Singh Raman, and C. C. Koch, "Bimodal grain size distribution: an effective approach for improving the mechanical and corrosion properties of Fe–Cr–Ni alloys," *Journal of Materials Science*, vol. 47, no. 22, pp. 7735–7743, 2012.

[38] E. McCafferty, *Introduction to Corrosion Science*, Springer, 2000.

[39] X. Huang, N. Tsuji, N. Hansen, and Y. Minamino, "Microstructural evolution during accumulative roll-bonding of commercial purity aluminum," *Materials Science and Engineering A*, vol. 340, no. 1-2, pp. 265–271, 2003.

[40] J. Čížek, I. Procházka, M. Cieslar et al., "Thermal stability of ultrafine grained copper," *Physical Review B—Condensed Matter and Materials Physics*, vol. 65, Article ID 094106, 2002.

[41] V. Y. Gertsman and R. Birringer, "On the room-temperature grain growth in nanocrystalline copper," *Scripta Metallurgica et Materiala*, vol. 30, no. 5, pp. 577–581, 1994.

[42] S. Komura, Z. Horita, M. Nemoto, and T. G. Langdon, "Influence of stacking fault energy on microstructural development in equal-channel angular pressing," *Journal of Materials Research*, vol. 14, no. 10, pp. 4044–4050, 1999.

[43] X. Molodova, G. Gottstein, M. Winning, and R. J. Hellmig, "Thermal stability of ECAP processed pure copper," *Materials Science and Engineering: A*, vol. 460-461, pp. 204–213, 2007.

[44] C. Sun, Y. Yang, Y. Liu et al., "Thermal stability of ultrafine grained Fe-Cr-Ni alloy," *Materials Science and Engineering A*, vol. 542, pp. 64–70, 2012.

[45] K. Neishi, Z. Horita, and T. G. Langdon, "Grain refinement of pure nickel using equal-channel angular pressing," *Materials Science and Engineering A*, vol. 325, no. 1-2, pp. 54–58, 2002.

[46] F. J. Humphreys, "A unified theory of recovery, recrystallization and grain growth, based on the stability and growth of cellular microstructures—I. The basic model," *Acta Materialia*, vol. 45, no. 10, pp. 4231–4240, 1997.

[47] V. Y. Gertsman, R. Birringer, R. Z. Valiev, and H. Gleiter, "On the structure and strength of ultrafine-grained copper produced by severe plastic deformation," *Scripta Metallurgica et Materiala*, vol. 30, no. 2, pp. 229–234, 1994.

[48] R. K. Islamgaliev, F. Chmelik, and R. Kuzel, "Thermal stability of submicron grained copper and nickel," *Materials Science and Engineering: A*, vol. 237, no. 1, pp. 43–51, 1997.

[49] C. H. Moelle and H. J. Fecht, "Thermal stability of nanocrystalline iron prepared by mechanical attrition," *Nanostructured Materials*, vol. 6, no. 1–4, pp. 421–424, 1995.

[50] J. R. Davis, *Stainless Steels*, ASM International, 1994.

[51] J. Horvath and H. H. Uhlig, "Critical potentials for pitting corrosion of Ni, Cr–Ni, Cr–Fe, and related stainless steels," *Journal of the Electrochemical Society*, vol. 115, no. 8, pp. 791–795, 1968.

[52] K. D. Ralston, N. Birbilis, and C. H. J. Davies, "Revealing the relationship between grain size and corrosion rate of metals," *Scripta Materialia*, vol. 63, no. 12, pp. 1201–1204, 2010.

[53] R. K. Gupta, R. K. Singh Raman, and C. C. Koch, "Electrochemical characteristics of nano and microcrystalline Fe–Cr alloys," *Journal of Materials Science*, vol. 47, no. 16, pp. 6118–6124, 2012.

[54] R. A. Andrievski, "Review stability of nanostructured materials," *Journal of Materials Science*, vol. 38, no. 7, pp. 1367–1375, 2003.

[55] C. C. Koch, "Structural nanocrystalline materials: an overview," *Journal of Materials Science*, vol. 42, no. 5, pp. 1403–1414, 2007.

[56] Q. Song, R. C. Newman, R. A. Cottis, and K. Sieradzki, "Validation of a percolation model for passivation of Fe-Cr alloys. Two-dimensional computer simulations," *Journal of the Electrochemical Society*, vol. 137, no. 2, pp. 435–439, 1990.

[57] K. Sieradzki and R. C. Newman, "A percolation model for passivation in stainless steels," *Journal of the Electrochemical Society*, vol. 133, no. 9, pp. 1979–1980, 1986.

[58] Y. R. Kolobov, G. P. Grabovetskaya, M. B. Ivanov, A. P. Zhilyaev, and R. Z. Valiev, "Grain boundary diffusion characteristics of nanostructured nickel," *Scripta Materialia*, vol. 44, no. 6, pp. 873–878, 2001.

[59] R. Würschum, S. Herth, and U. Brossmann, "Diffusion in nanocrystalline metals and alloys—a status report," *Advanced Engineering Materials*, vol. 5, no. 5, pp. 365–372, 2003.

[60] E. M. Gutman, *Mechanochemistry of Solid Surfaces*, World Scientific, Singapore, 1994.